Effect of gas tungsten arc welding parameters on surface morphology and wear behavior of stellite 12 coating on Inconel 625

V. Klishadi, M. Kasiri-Asgarani, M. Naalchian, E. Ebrahimi-Kahrizsangi, H.R. Bakhsheshi-Rad

Advanced Materials Research Center, Department of Materials Engineering, Najafabad Branch, Islamic Azad University, Najafabad, Iran

Abstract

In this research, the microstructure, hardness and wear behaviour of stellite 12 coated Inconel 625 nickel-based superalloy were investigated. Gas tungsten arc welding (GTAW) with a current intensity of 90 and 120 Am in one, two and three passes was used for coating. An optical microscope, electron microscope with EDX elemental analysis, phase analysis with X-ray diffraction (XRD), hardness test and wear test were used to evaluate the coating performance. The interface of the stellite coating/Inconel 625 in all samples was free of any cracks and holes and a proper connection was formed. The microstructure of the stellite coated mainly consists of cobalt-rich γ phase in the dendrite structure with a network of Cr_7C_3 and $Cr_{23}C_6$ carbides in the inter-dendritic regions, as well as M_6C and M_3C complex carbides such as $(Co,W)_6C$, Co_6Mo_6C, Co_3Mo and Co_3W. The presence of carbide particles along with the reduction of input heat increased the hardness of the stellite coatings. The range of increased hardness of the cross-sections of the stellite coated samples was measured between 422 and 1221 HV, while the hardness value of the uncoated sample was about 335 HV. By formation of stellite 12 coating layer on surface of Inconel 625, the wear behaviour improved while its effectiveness significantly decreased with the reduction of heat input. The wear mechanism of uncoated and stellite 12 coated samples was also evaluated and discussed in the present study.

Keywords: Inconel 625, Stellite 6, coating, microstructure, hardness, wear behavior.

1. Introduction

Nickel chrome alloy 625 is widely used in various industries due to its high tensile strength, high creep and tear strength, extreme fatigue strength, oxidation and corrosion resistance, and excellent welding and soldering ability. This alloy is used in power plants and heat exchangers, harness cables, aeroplane propeller blades, and submarine propulsion engines. However, despite all these characteristics, this super alloy has a less significant wear resistance, particularly at high temperatures [1]. Stellite superalloys are mainly composed of cobalt-based alloys and a combination of cobalt-chromium alloys. These alloys also contain tungsten or molybdenum with less than 3 wt.% carbon. Stellite alloys are generally strengthened by the precipitation of carbides in the matrix of cobalt solid solution. Excellent tribological properties, favourable mechanical strength, excellent resistance to loading under static conditions, fatigue and creep, suitable surface stability, high resistance to corrosion and oxidation, and good phase stability at high temperatures are the main characteristics of stellite alloys. The existence of these characteristics justifies its use as a coating to protect metals and other alloys [1]. Deng et al. [2] coated the surface of shafts fabricated from martensitic stainless steel with cobalt base alloy powder Satelite 12 by plasma arc welding process to improve the surface properties. They found that the interface between the

coating and the based metal is free of cracks and holes. As the distance from the interface increases, the HAZ shows three microstructural zones: coarse grain, tempered martensite, and martensite-ferrite. The coating microstructure mainly consists of cobalt-rich γ phase in the dendrite structure with a network of Cr_7C_3 and $Cr_{23}C_6$ chromium carbides in the inter-dendritic regions [2]. Huiji Shi et al. coated the surface of said steel with cobalt-base alloy powder stellite 12 by the plasma arc welding process to evaluate the effect of coating thickness and temperature on the mechanical properties of DIN X45CrSi9-3 heat-resistant martensitic steel. Their result exhibited that the decrease in the thickness of the coating from 2.5 mm to 1 mm did not cause a big drop in the hardness of the coating and in the bending strength of the samples, but increasing the temperature from the ambient temperature to 500 ^oC caused a significant decrease in the bending strength of the sample [3]. Yourong et al [4] also coated the stellite 12 alloy powder by CO_2 laser welding process on a based metal fabricated from T8 tool steel. They investigated the effect of laser speed on the phase chemical composition, microstructure, microhardness and wear resistance of the coated steel. Phase analysis result showed that the coated layer consisted of a mixture of supersaturated solid solution phase (Co, Cr) γ and compact hexagonal carbide M_7C_3. The main factor in improving wear resistance was the precipitation of M_7C_3 complex carbide, while the increase in microhardness is achieved by increasing the solubility of supersaturated elements in the (Co, Cr) γ matrix phase. Promdirek et al [5] investigated the effect of GTAW parameters on the high temperature corrosion-wear resistance of Inconel 800 coated by Stellite 12. Their result exhibited that high welding speed leads to the formation of finer dendrites. The results also revealed that the hardness increases with the decrease in the size of the dendrites. However, the effect of current intensity and the number of coating passes of stellite 12 on the microstructure and surface properties of Inconel 625 by GTAW process have not been investigated elsewhere. Therefore, the purpose of this research is utilizing stellite 12 powder as a coating layer using GTAW to enhance mechanical properties and wear resistance of Inconel 625 nickel-based super alloy.

2. Materials and methods

Inconel 625 nickel superalloy was used as a substrate and its chemical composition was presented in Table 1. This alloy contains significant amounts of elements such as chromium, molybdenum and niobium, which improve mechanical and wear properties of the Inconel 625. Cobalt based-alloy powder stellite 12 used for surface treatment contain primary particle size of 40 to 80 μm (French Estel Oric Company) possess chemical composition which also listed in Table 1 used for surface alloying. Then this powder was subjected in planetary ball mill under condition of Al_2O_3 as ball material along with ball-powder weight ratio of 5:1, and mass of powder of 10 gr. the milling process continue until the size of the resulting powder particles reached in the range of 20 to 40 μm.

Table 1 Chemical compositions of the Inconel 625 and stellite 12

Element (wt.%)	**Cr**	**Si**	**Nb+Ta**	**Mn**	**Mo**	**C**	**Fe**	**Ni**
Compositions of Inconel 625	21.7	0.06	3.5	0.04	8.6	0.02	0.3	Bal.
Element (wt.%)	**C**	**Si**	**Cr**	**Ni**	**Mo**	**W**	**Fe**	**Co**
Compositions of stellite 12	1.8	1.3	29	<3	<1	9	<2	Bal.

Square plates with dimensions of 10×50×50 mm^3 were cut from Inconel 625, and to facilitate sticking the powder with the desired alloy composition on the surface, grooves with dimensions of 5×20×20 mm^3 were formed in the middle of these square plates with a milling machine (SMG-300). The sample was washed thoroughly with running distilled water, rinsed and ultrasonically degreased with acetone and dried. Then the alloy powder with adhesive (polyvinyl alcohol) and distilled water with a ratio of 1 to 3 and a ratio of powder to binder of 10 were thoroughly mixed in the mill, and after it became a paste, it was placed inside the groove with a uniform thickness. GTAW parameters for stellite 12 coating Inconel 625 listed in Table 2, the effect of changes in current intensity and number of passes was investigated. The welding torch was moved by a movable table in the X and Y axes at a constant speed of 70 mm/min on the surface of the sample. The glued samples were subjected to a temperature of 450 ^oC for 60 min before welding in order to evaporate the PVA glue and preheat. After completing the welding operation, in order to prevent the appearance of cold cracks, the samples were placed inside the furnace with a temperature of 450 ^oC and cooled slowly.

Table 2 GTAW parameters for stellite 12 coating Inconel 625

No. Sample	Input heat (kJ/mm)	Number of pass	Speed (mm/ min)	Type of polarity	Protective gas rate (Lit/min)	Type of protective gas	Voltage (V)	Current intensity (A)	Amount of powder (gr)
1	28.10	1	70	DCEN	5	Argon	13	90	10
2	28.10	2	70	DCEN	5	Argon	13	90	10
3	28.10	3	70	DCEN	5	Argon	13	90	10
4	37.13	1	70	DCEN	5	Argon	13	120	10
5	37.13	2	70	DCEN	5	Argon	13	120	10
6	37.13	3	70	DCEN	5	Argon	13	120	10

Note: No coating parameters for bare Inconel 625

Microstructure of the samples prepared from the working surface and spalling specimen was characterized via optical (OLYMPUS BH-2 VEGA) equipped with imager analyzer (Clemex) and scanning electron microscopes (SEM; TESCAN-LMU) equipped with energy dispersive spectrometry (EDS), while microhardness value of the samples was measured by Vickers hardness testing (Zwick model ZHU250) method using 30 kg force. Five indentations were carried out on each specimen to attain an average value of microhardness. For microstructural examination of phases, the specimens were etched in 20ml HCL+1ml H_2O_2 (30%) for 20 s. X-ray diffractometry (Siemens-D500) was used to evaluate phases present in the specimens by using Cu-Kα line generated at 40 kV and 35 mA. Wear tests were evaluated by a pin-on-disk tribometer, according to the ASTM G99-95A standard. For this purpose, samples in the form of pins with a diameter of 5 mm were prepared and subjected to wear in dry conditions and room temperature, with an applied load of 10 N, a speed of rotation of the disk of 350 rpm and a distance of 1000 m, and then the amount of the worn weight of the samples with the accuracy of 0.0001 gr was measured.

3. Results and discussion

3.1. Microstructure

Fig. 1 shows optical microstructures of the stellite coated surface samples according to the conditions of Table 2. As can be seen, as the welding current increases, the heat input to the work piece increases and the cooling rate decreases, which causes the dendritic arms to become larger. Also, by increasing the number of stellite coating passes with similar current intensity, the structure of the samples became coarser and more discontinuous. Coarsening of the microstructure with

increasing current intensity shows the relationship between the average input heat and the intensity of dendrite nucleation and the growth rate during welding [6]. For the intensity of low currents, the cooling rate due to the high thermal gradient in the melt is higher, as a result, more nuclei's are allowed to grow. Higher intensity of sprouting leads to the shortening of dendritic arms and causes the appearance of larger amounts of inter-dendritic area. On the contrary, a higher current intensity leads to an increase in the growth rate along with the thickening of the dendritic arms, because the cooling rate decreases due to more heat input to the part. Therefore, dendritic arms become thicker when the current intensity increases [7, 8]. The average size of dendritic arms and the distance between dendritic arms near the surface for stellite 12 coated samples are presented in Table 3. As can be seen, with increasing the number of passes and when same current intensity applied for all samples, the structure became coarser and more discontinuous, because with escalating of passes number, the thermal gradient and solidification rate decreased. Under the influence of relative remelting and input heat caused by applying the next pass on the lower layers, the dendrites of the first layers have thickened. It is worth noting that the cooling rate is higher in the upper layers, hence, the dendrites in the adjacent areas of the surface is finer and thinner. The greater fineness of the dendrites near the surface is the result of the faster cooling rate due to more exposure of the surface to the air. These results are consistent with the research conducted by Liu [9], which employed the coating of stellite cobalt base alloys 3, 6 and 12 on the martensitic steel and found that the structure became finer from the interface to the surface of the stellite coating.

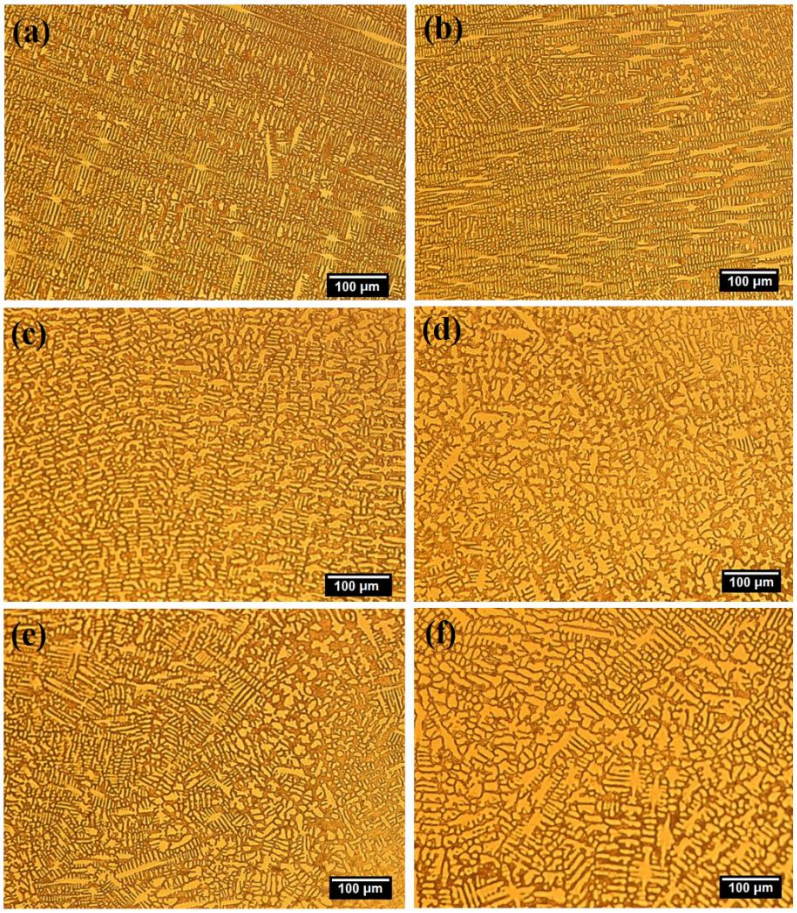

Fig. 1. Surface microstructure of stellite 12 coated on the substrate, (a) sample 1, (b) sample 2, (c) sample 3, (d) sample 4, (e) sample 5, (f) sample 6

Table 3 The average size of grains in the dendritic region, the average distance from the center to the center of dendrites and inter-dendritic spaces

No. Sample	Average interdental spaces (%)	Average distance from center to center of dendrites (µm)	Average size of dendrites (μm^2)
1	40	3	93
2	31	5	99
3	29	6	134
4	28	6	139
5	23	7	144
6	16	9	148
IN 625	-	-	137

Fig. 2 shows the images of the microstructure of the cross-section of the substrate near the interface and the stellite coating formed on the surface sample 2. The absence of cracks and holes in the interface between the substrate and the coating indicates the effectiveness of this coating. The interface has a strong metallurgical bond that connects with substrate. Due to the high solidification rate and high thermal gradient, the interface provides the conditions for formation of great adhesive strength between stellite layer and substrate in short duration by solidifying the coating and creating the penetration zone at the same time. A high concentration gradient in the interface leads to a strong penetration of the soluble element from the coating to the substrate and vice versa, which has resulted in high bonding strength between the based-metal and the coating. After the melting of a part of the substrate and the complete melting of the coating, solidification started. The interface coating/substrate has a high solidification rate due to the presence of melt on the interface and the contact with the substrate. As a result of melting of the substrate, this area has the highest concentration of nickel and the lowest concentration of carbon and chromium. Fig. 2 also shows the structural changes of the dendrites in sample 2 from near the interface coating/substrate. As can be observed, the distance between the arms of dendrites change throughout the melting zone, such as the solidification condition. Since the cooling rate in the welding line is higher than the melting line, the distance between the arms of the dendrites decreases from the melting line to the welding center line. In general, with increasing cooling rate, the distance between dendritic arms decreases. Therefore, as can be seen in Table 4, the dendritic structure is coarser near the substrate interface, and the dendrites are finer as they move towards the coated layer. These findings are consistent with the results of Murphy's study [10].

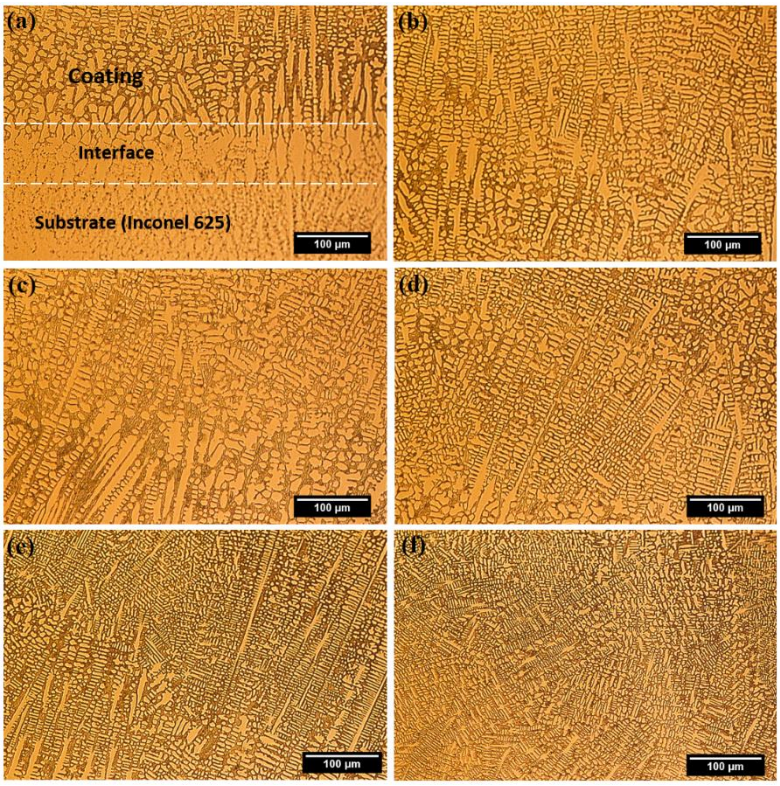

Fig. 2. The microstructure of the cross-section of the substrate near the interface and the coating for sample 2, (a) the interface of the substrate and the coating, (b) slightly above the interface of the coating/substrate, (c) the beginning of the formation of equiaxed dendrites, (d) equiaxed dendrites become finer by moving away from the interface, (e) near the welding crown top zone, (f) welding crown top zone

Table 4 Size variation of primary and secondary dendrites for coated samples

Sample	Width of secondary dendritic arms (µm)	Length of secondary dendritic arms (µm)	Width of primary dendritic arms (µm)	Length of primary dendritic arms (µm)
1	3	6	6	76
2	4	7	7	82
3	7	11	9	115
4	4	7	8	77
5	5	9	10	98
6	7	11	11	126

Fig. 3a-c shows the microstructure changes from the interface to the weld surface of sample 1. This area consists of columnar dendrites in different directions and the area of equiaxed dendrites near the coating surface. During welding, when the chemical composition and crystal structure of the base metal and the weld metal are the same, hence the epitaxial growth occurred. This means that the grain boundary was formed along the internal grain boundary of the based metal and then grew in a direction perpendicular to the weld interface towards the weld metal [10]. In the same manner, because Inconel 625 has an austenitic structure with the FCC structure and stellite 12 likewise has the FCC structure, as a result, epitaxial growth can be observed at the interface between the base metal and the weld metal. During solidification of the cladding metal, grains tend to grow in the direction perpendicular to the weld pool boundary. The reason for this is the existence of the highest thermal gradient and, as a result, the highest heat output in this direction

[10]. Plane growth pattern can be reported near the interface. This pattern can be seen as a result of high temperature gradient and low combined solidifying along the solid-solution interface [8]. The planar region has also been observed in many other studies conducted in the field of hardening of stellite layers deposited by various welding processes [11, 3, 5]. In general, the solidify microstructure for each coated sample includes dendritic and interdendritic regions, which is clearly shown in Fig. 3d.

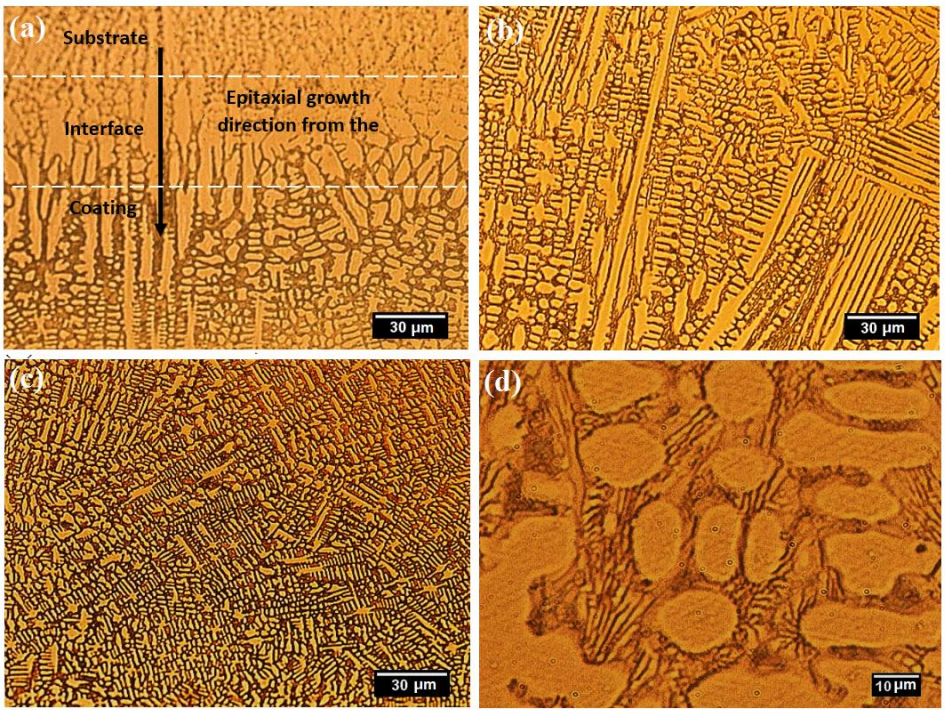

Fig. 3. The microstructure of the cross- section of the substrate from the vicinity of the interface to the coating for sample 1, (a) epitaxial growth in the planar region, (b) competitive growth of columnar dendrites, (c) region of fine equiaxed dendrites and (d) the cross-sectional image of structure of coated sample 5

Fig. 4 shows the SEM image and corresponding EDS analysis of dendrites and inter-dendritic areas in sample 1. The microstructure depends on the solidification process. The remaining melt is transformed into a dendritic mixture of cobalt-rich phase and carbide phases (brittle phase) by a eutectic reaction. During solidification, the separation of chromium may be favorable for the precipitation of chromium-rich carbides in the interdendritic regions such as: Cr_7C_3 and $Cr_{23}C_6$ [13-15]. The microstructure includes dendritic matrix with light gray color (area A) and compounds appearing in dark gray (area B) and white (area C) in layered morphology. EDS analysis also shows that the dendritic matrix of stellite 12 coating (area A) basically includes cobalt and chromium with a small amount of tungsten and nickel. While the dark gray compounds (part B) are identified by their high chromium content, the white part (area C) mainly consists of cobalt, chromium, tungsten and molybdenum. The EDS analysis of stellite 12 coating shows that a small amount of molybdenum is dissolved in the dendritic matrix, and dark gray compounds (~3 at.%) and white compounds are significantly enriched in molybdenum (~7 at.%).
Due to the low solubility of molybdenum in the cobalt-rich solid solution phase, molybdenum is mainly found in the interdendritic region. The matrix with a light gray color in the microstructure

of the stellite 12 coating (part A) as a solid solution (FCC) of α-Co is identified. Due to their high chromium content, the dark gray compounds as a network of Cr_7C_3 and $Cr_{23}C_6$ chromium carbides in the inter-dendritic regions are identified. White compounds due to the presence of high amounts of tungsten and molybdenum in the form of M_6C complex carbides; containing tungsten $(Co,W)_6C$ and molybdenum (Co_6Mo_6C) as well as intermetallic compounds containing molybdenum (Co_3Mo) and tungsten (Co_3W) are identified [49]. In addition to the aforementioned compounds, intermetallic compounds containing tungsten (Co_3W and Co_7W_6) as well as complex carbides containing tungsten (Co_3W_3C and Co_6W_6C) and molybdenum have been identified [3-5, 11, 12]. These carbides are not detected by the XRD analysis due to the presence of small amount of the carbides in the stellite 12 coating.

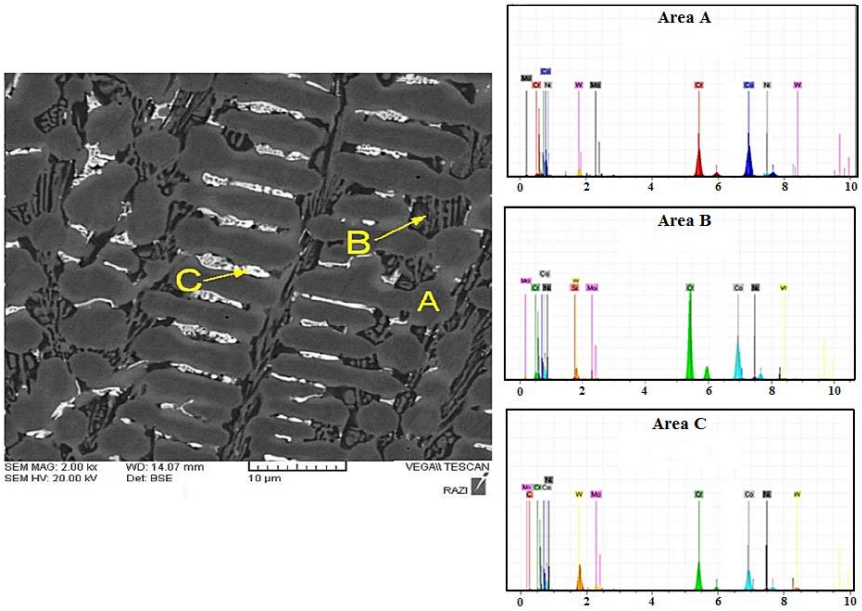

Fig. 4. SEM image and corresponding EDS analysis of cross-sectional structure of stellite 12 coating on Inconel 625 (sample 1)

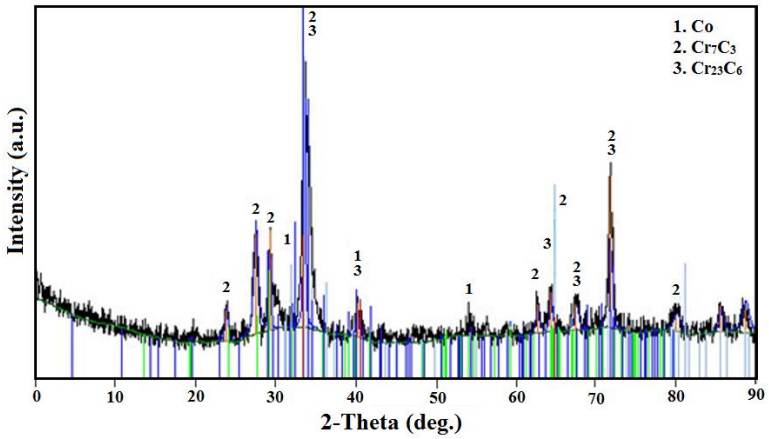

Fig. 5. XRD pattern of stellite 12 coating on Inconel 625

Fig. 6 show line scan across the SEM image of samples 1 and 3. As can be obvious, in the single-pass sample, the dilution of nickel in the created stellite coating is high, but in the 3-pass sample, this amount is very low. In fact, in the three-pass sample, due to the effect of the second and third

layers and the resulting heating and remelting of the first layer, the influence of the chemical composition of the substrate on the distribution of the alloy elements of the deposited layer has decreased and the role of the stellite 12 alloy has increased. In both samples, it can be seen that small amounts of cobalt, carbon and tungsten have penetrated from the stellite coating into the substrate, and the contribution of cobalt and tungsten is higher, therefore, due to the high contribution of these elements in the composition of stellite 12 alloys, dilution It seems self-evident through penetration into the substrate.

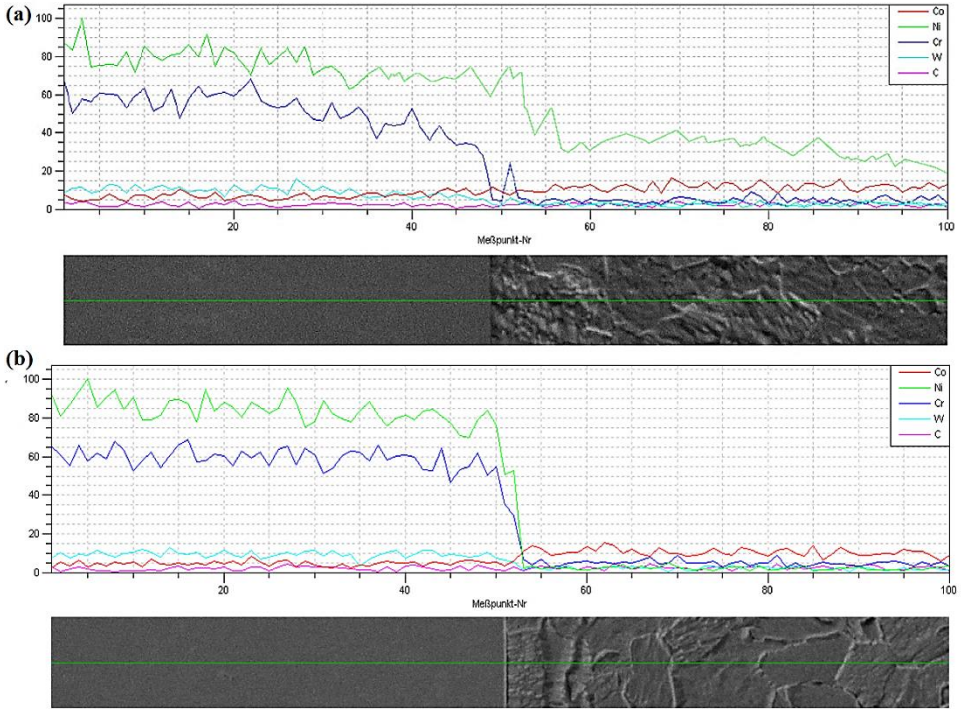

Fig. 6. Line scan across the SEM image of (a) samples 1 and (b) sample 3

3.2. Hardness profile measurement

The results of surface hardness of the samples are presented in Table 5. As can be seen, the surface hardness of the substrate is significantly lower than the surface hardness of the stellite coated samples. The result also indicated that the surface hardness of single pass, two pass and three pass samples with currents of 90 and 120 Am; the surface hardness decreases with the increase of current intensity. It should also be noted that as the number of passes increases, the surface hardness decreases when the current intensity is similar. The hardness results have a good consistency with other published results [45].

Table 5 Hardness profile of Inconel 625 and stellite coated samples

Sample	IN 625	Sample 1	Sample 2	Sample 3	Sample 4	Sample 5	Sample 6
Hardness (HV)	175±4	482±10	470±10	453±9	427±9	395±8	378±7

Fig. 7 shows the Vickers microhardness profile for the cross-section of the stellite coated samples from the based metal to the stellite coating surface. As can be seen, the hardness of the based metal is almost constant and its average value is 355 HV. It can be concluded that the carbide deposition in the area near the interface of the stellite coating/substrate is low, especially along the interface. As a result, the hardness decreases in the area near the interface, and by moving away from this

area and moving towards the surface of the coating, the hardness increases with the formation of a dendritic structure with fine grains and the deposition of more carbides. In addition, it is observed that hardness value has decreased in the coarse grain area near the interface of coating/substrate. The reason for the gradual drop in hardness value at the interface is the dilution effect caused by the partial melting of the substrate. Since the formation of the stellite coating occurred at a high speed and there is the possibility of remaining residual stresses in the stellite coating; the penetration of the substrate and the gradual decrease in hardness caused an increase in adhesive strength and a decrease in the brittleness of the stellite coating which consider as a favorable factor that can prevent the occurrence and growth of cracks in the stellite coating. On the other hand, in this area, first a planar area and then a dendritic structure with a relatively large size of primary dendrites are observed [7-11].

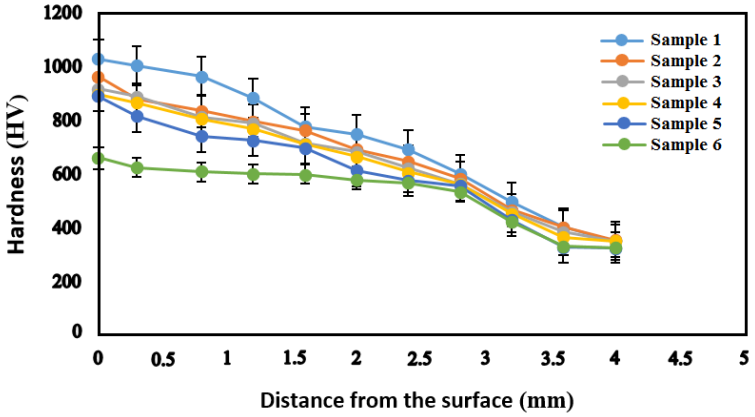

Fig. 7. Hardness profile as a function of distance from the surface of stellite 12 coated Inconel 625

3.3 Wear behavior

Fig. 8 shows the graphs of the friction coefficient according to the sliding distance for stellite 12 coated and uncoated Inconel 625 samples. According to the friction coefficient curves, the average friction coefficient is presented in Table 6. As can be seen, the lowest friction coefficient is related to sample 6 and the highest friction coefficient and maximum value of weight loss are related to Inconel 625 sample, so it can be concluded that sample 6 with has the highest wear resistance and the lowest amount of weight loss after the wear test. By evaluating the graphs of the friction coefficient according to the sliding distance and examining the width of the worn surfaces in the SEM images, the lowest friction coefficient, weight loss and worn width, which indicates the highest wear resistance is related to sample 6, however, sample 1 presented highest hardness value. The reason for this should be found in the heterogeneity of the microstructure. Due to the lower input heat in the sample with the lowest current intensity, more brittle phases (carbides) are formed in the inter-dendritic regions in the structure. Therefore, more amounts of brittle phases are removed during friction due to dry wear and ultimately the surface scratch is intensified. On the other hand, in samples with 3 passes, the structure is thicker and more heterogeneous compared to samples with fewer passes, or in other words, the dendrites are distributed in a larger volume of space, and as a result, the carbides in the inter-dendritic spaces in the microstructure are more complex and compact, because the temperature gradient and freezing speed decrease as the number of passes increases. The obtained results are consistent with the findings given in references.

Fig. 9 shows the SEM image of the wear surface of sample 6, sample 2 and Inconel 625 based-metal after performing the wear test. In the wear surface of sample 6, the traces of scratches and spalling are rarely observed only in the specified part on the surface. However, the several scaraches and layered structure and also the color change of the surface can be seen, so the dominant mechanism of wear is adhesive wear (Fig. 9a). The wear surface of sample 2 shows more signs of blunting and plastic deformation than sample 6, which is caused by the presence of a larger amount of carbides in the inter-dendritic spaces (Fig. 9b). Inconel 625 base metal has the higher friction coefficient including larger porosities, grooves and wear debries compared to the coated samples (Fig. 9c). In the figure, the effects of material movement next to the void which formed on the surface can be seen. The presence of grooves on both sides of which there are protrusions of the coated material, shows that besides adhesive wear, the dominant wear mechanism for this sample is abrasive wear. This mechanism occurs when the surface of the pin is much smoother than the abrasive disc.

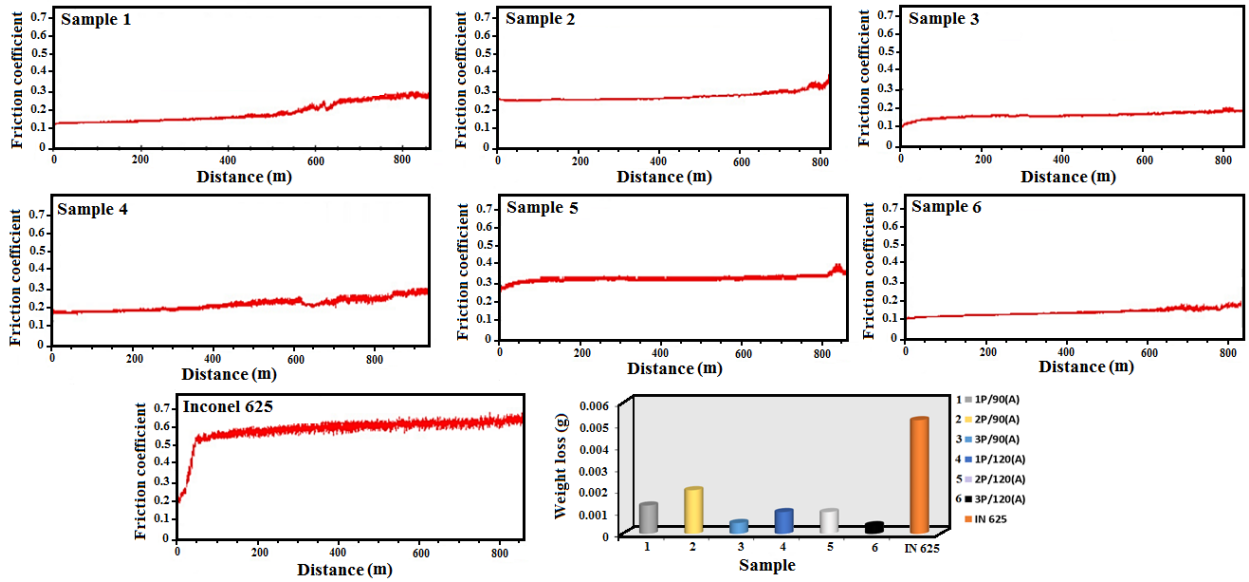

Fig. 8 (a) The graphs of the friction coefficient as a function of the sliding distance for uncoated Inconel 625 and stellite coated samples (b) Weight loss of the uncoated Inconel 625 and stellite coated samples after the wear test

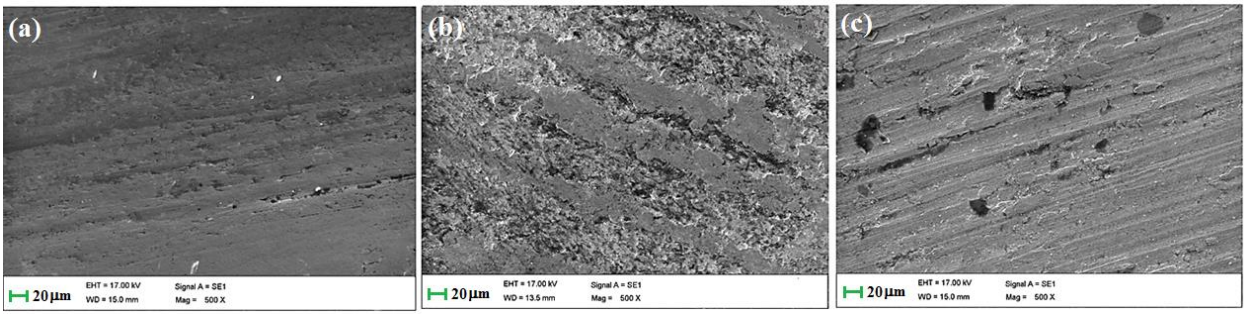

Fig. 9. SEM image of the wear surface of a) sample 6, b) sample 2 and c) Inconel 625 based metal after the wear test

Table 6 Friction coefficient as a function of the sliding distance for uncoated Inconel 625 and stellite coated samples

Sample	IN 625	Sample 1	Sample 2	Sample 3	Sample 4	Sample 5	Sample 6
Friction coefficient (μ)	0.62±0.05	0.26±0.05	0.34±0.05	0.16±0.05	0.28±0.05	0.36±0.05	0.15±0.05

4. Conclusions

In this study, stellite 12 coating was prepared on the surface of Inconel 625 nickel-based superalloy by gas tungsten arc welding (GTAW), and subsequently its surface morphology and wear properties were investigated. The results of this research are presented as follows:

1. The interface of the stellite 12 coating with the substrate is free of any cracks and holes. In addition, by preparation of the stellite 12 coating formed on Inconel 625, the hardness value of the surface increases from 175 to 480 HV.

2. The stellite 12 coating microstructure mainly consists of cobalt-rich γ phase in the dendrite structure with a network of Cr_7C_3 and $Cr_{23}C_6$ chromium carbides in the inter-dendritic regions, as well as intermetallic compounds containing M_6C and M_3C complex carbides such as $(Co,W)_6C$), Co_6Mo_6C, Co_3Mo and Co_3W.

3. As the current intensity and subsequently heat input decreases, the hardness value increases due to the fineness of the stellite 12 coating microstructure. Moreover, the wear behavior of the stellite 12 coatings was improved by reducing the volume fraction of carbides in the inter-dendritic spaces. The wear mechanism in the uncoated Inconel 625 sample is abrasive wear, while the dominant wear mechanism for stellite 12 coating is adhesive wear.

References

[1] Kapoor.S, Liu.R, Wu. X.J, Yao. M.X, "Temperature-Dependence of Hardness and Wear Resistance of Stellite Alloys", International Journal of Chemical, Molecular, Nuclear, Materials and Metallurgical Engineering, Vol.6(7), pp. 592- 601, 2012.

[2] Deng. D.W, Zhang. C.P, Chen. R, Xia. H, "Microstructure and microhardness of 17-4PH deposited with Co-based alloy hardfacing coating", Physics Procedia, Vol. 50, pp. 177- 184, 2013.

[3] Deng. H, Shi. H, Tsuruoka. S, "Influence of coating thickness and temperature on mechanical properties of steel deposited with Co-based alloy hardfacing coating", Surface & Coatings Technology, Vol. 204, pp. 3927-3934, 2010.

[4] Yourang. X.U, Hengua. ZH, Daming. CH, Fuchun. XI, Mingya. XU, "Effect of laser scannig speed on phase constitution ad wera resistance of laser cladding hardfacing alloy stellite 12", Acta Metallurgica Sinica(English Edition), Vol. 6, pp. 300-303, 1993.

[5] Promdirek. P, Chandra-ambhorn. S, Prasong. R, Rittirat. S, Pornpaisansakul. N, "Influence of gas tungsten arc welding parameters on thehigh-temperature erosion-corrosion resistance of Incoloy 800 cladded by Stellite 12 for the application as thermowell", Materials Science Foru, Vol 696 (2011) pp 248-253.

[6] D'Oliveira. A.S.C.M, Paredes. R.S.C and Santos. R.L.C, "Pulsed current plasma transferred arc hardfacing", Journal of Materials Processing Technology, Volume 171, Issue 2, pp. 167-174, 20 January 2006.

[7] Takano. E.H, Queiroz. D.D and D'Oliveira. A.S.C.M, "Evaluation of processing parameters on PTA hardfacing surfaces", Welding International, Volume 24, Issue 3, pp. 241-248, 2010.
[8] R. Arabi Jeshvaghani, M. Shamanian, M. Jaberzadeh, "Enhancement of wear resistance of ductile iron surface alloyed by stellite 6", Materials and Design, 32 (2011) 2028-2033.
[9] Liu. E, Wu. X.J, Kapoor. S, M.X. Yao, R. Collier, "Effects of Temperature on the Hardness and Wear Resistance of High-Tungsten Stellite Alloys", Metallurgical And Materials Transactions A, Volume 46A, pp. 598-599, 2015.
[10] Murphy. R.D.B, "Hardfacing As A Useful Repair Method", Dep. of Mechanical Engineering, Queensland Institute of Technology, 1973.
[11] Moradi. M.J, Ketabchi. M, "An experimental study of microstructure and mechanical mehavior of Alloy 625 Weld Overlay Deposited On ASTM A516 Grade 70", Indian Journal Of Science and Technology, Vol. 8(12), pp. 1-5, 2015.
[12] Motallebzadeh. A, Atar. E, Cimenoglu. E,"Sliding wear Characteristics of molybdenum containing Stellite 12 coating at elevated temperatures", 2th Tribology International, pp 1-13, 2015.
[13] Naalchian M, Kasiri-Asgarani M, Shamanian M, Bakhtiari R, Bakhsheshi-Rad HR. Effect of substrate's heat treatment on microstructure and mechanical properties TLP bonding of dissimilar X-45/FSX-414 cobalt based superalloys. Metals and Materials International. 2021:4657-68.
[14] Ghahferokhi AI, Kasiri-Asgarani M, Amini K, Ebrahimi-kahrizsangi R, Rafiei M. Evolution of microstructure and mechanical properties on dissimilar transient liquid phase (TLP) bonding of GTD-111 and IN-718 by BNi-9 (AWS A5. 8/A5. 8M) interlayer. Welding in the World. 2021;65(2):329-43.
[15] Hafizi M, Kasiri-Asgarani M, Naalchian M, Bakhsheshi-Rad HR, Berto F. The Effect of Holding Time on Dissimilar Transient Liquid-Phase-Bonded Properties of Super-Ferritic Stainless Steel 446 to Martensitic Stainless Steel 410 Using a Nickel-Based Interlayer. Micromachines. 2022: 22;13(11):1801.